# Investigation of a sandwich plate with two MEE face sheets and FGM core layer from the nonlinear dynamic buckling point of view

Ngo Dinh Dat
*Department of Engineering and Technology in Constructions and Transportation -University of Engineering and Technology, VNU Hanoi.*
ngodinhdat0405@gmail.com

Nguyen Dinh Duc
*Department of Engineering and Technology in Constructions and Transportation -University of Engineering and Technology, VNU Hanoi.*
ducnd@vnu.edu.vn

Vu Dinh Giang
*Faculty of Engineering Mechanics and Automation - University of Engineering and Technology, VNU Hanoi.*
rangsut2k@gmail.com

Vu Thi Thuy Anh
*Department of Engineering and Technology in Constructions and Transportation -University of Engineering and Technology, VNU Hanoi.*
anhvutt@vnu.edu.vn

***Abstract*: A sandwich plate with two Magneto-Electro-Elastic (MEE) face sheets and Functionally Graded Materials (FGM) core layer resting on an elastic foundation and in a thermal environment will be studied in this paper for the nonlinear dynamic buckling problem. The hypothetical plate model above is formed from the fact that MEE materials have been receiving special attention from the research community owing to their specialized performance and coupled behavior under thermal, electric, magnetic, and mechanical loads, while FGM has been introducing for controlling material response to deformation, dynamic loading as well as to corrosion and wear, etc. The combination of these two materials in the sandwich plate model is expected to create a remarkable new sandwich model. The establishment of all basic equations for the nonlinear dynamic buckling problem of this novel sandwich model will be solved by analytical methods, and the effects of geometrical parameters, temperature, electric and magnetic potentials on the nonlinear dynamic buckling of the sandwich plate will be shown in the numerical results of this study.**

***Keywords:*** *Smart materials, MEE, FGM, plate, dynamic, vibration, analytical method.*

## I. INTRODUCTION

Many applications such as aerospace, automotive, power generation, microelectronics, structural, and bio-engineering demand properties that are unobtainable in conventional engineering materials. These applications require mutually exclusive properties to have resistance against thermo-mechanical stresses as well as chemical stability. The need for property distributions is found in a variety of common products that must have multiple functions, such as gears, which must be tough enough inside to withstand the fracture but must also be hard on the outside to prevent wear. similarly, a turbine blade should also possess a property distribution; the blade must be tough to withstand the loading, but it must also have a high melting point to withstand high temperatures on the outer surface...

MEE material is a new material that shows the full coupling between magnetic, electric, elastic fields, and the magneto-electric effect. In which, the magneto-electric effect is the phenomenon where a magnetic polarization occurs due to an electric field and vice versa. It is thanks to these properties that MEE is seen to be a smart material that has the ability to change reversibly their properties to respond to external environments such as stress, temperature, moisture, electric or magnetic fields. MEE has received considerable interest because of a wide variety of applications in sensors, civil structures, aerospace control systems, and medical devices [1].

Also, considered a new type of material, FGM exhibits many advantages compared to conventional alloys and composite materials. FGM may be used by the variation in composition and structure fought over volume, resulting in corresponding changes in the properties of the material, or otherwise, FGM gives the opportunity to take the benefits of different material systems e.g. ceramics and metals, simultaneously provide a thermal barrier and reduced residual stress coating [2].

If the experimental studies are not included, the theoretical studies of material can be divided into two groups: research by numerical methods and research by an analytic method. Each method has its own advantages and disadvantages. For the analytical method, the equations and the computation process will become very complex. However, the benefits of this method were that the obtained results are explicitly stated in terms of the input parameters of the material and the structure, so when we change these parameters, we can actively control the behaviors of the structures.

Research on MEE or FGM has received a lot of attention from scientists, including the authors or groups such as [3-10]. However, studies on MEE or FGM sandwich structure are still very limited. Some studies can be mentioned such as [11-13]. It is easy to see that most of the research mentioned above is solved by the numerical method, while the number of studies is solved by analytic methods is very limited. So, this suggests that more research on sandwich structures is still needed.

By using an analytical method based on classical plate theory, the report focuses on studying the nonlinear dynamic buckling of the sandwich plate with two MEE face sheets and FGM core layer subjected to the combination of external pressure, thermal, electric, and magnetic loads. In addition to the numerical survey results, the comparison results are also shown in the results section to assess the reliability of the research method in the article.

## II. MATHEMATICAL MODEL

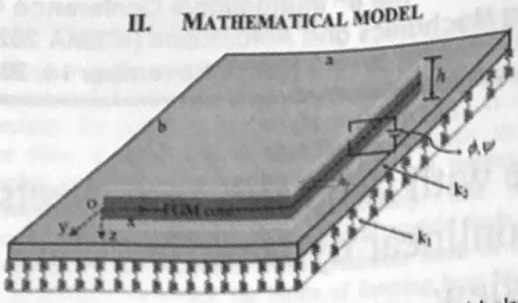


Fig. 1. The configuration and coordinate system of the sandwich plate

Consider a sandwich plate with two MEE face sheets and FGM core layer resting on elastic medium and subjected to the combination of external pressure, thermal, electric and magnetic loads with the size of the plate $a \times b \times h$ as shown in Fig. 1. A coordinate system $(x, y, z)$ is established in which $(x, y)$ plane on the middle surface of the sandwich plate and $z$ on thickness direction.

### A. Mechanical properties of MEE face sheets

TABLE I. MECHANICAL PROPERTIES OF MEE MATERIAL.

| Material properties | Notation | Values |
|---|---|---|
| Elastic constants $(GPa)$ | $C_{11}^f = C_{22}^f$ | 220 |
| | $C_{12}^f = C_{13}^f = C_{23}^f$ | 120 |
| | $C_{33}$ | 215 |
| | $C_{44} = C_{55}$ | 45 |
| | $C_{66}$ | 0 |
| Piezoelectric constants $\left(C/m^2\right)$ | $e_{31}$ | −3.5 |
| | $e_{33}$ | 9.0 |
| | $e_{15}$ | 0 |
| Dielectric constants $\left(C/\mathrm{N}m^2\right)$ | $\eta_{11} = \eta_{22}$ | $0.85\times10^{-9}$ |
| | $\eta_{33}$ | $6.3\times10^{-9}$ |
| Magnetic permeability $\left(\mathrm{Ns}^2/C^2\right)$ | $\mu_{11} = \mu_{22}$ | $-2\times10^{-4}$ |
| | $\mu_{33}$ | $0.9\times10^{-4}$ |
| Piezomagnetic constants $(N/\mathrm{A}m)$ | $q_{31}$ | 350 |
| | $q_{33}$ | 320 |
| | $q_{15}$ | 200 |
| Magneto-electric constants (Ns/VC) | $m_{11} = m_{22}$ | $5.5\times10^{-12}$ |
| | $m_{33}$ | $2600\times10^{-12}$ |
| Pyroelectric constant $\left(C/m^2K\right)$ | $p_3$ | $7.8\times10^{-7}$ |
| Pyromagnetic constant $\left(C/m^2K\right)$ | $\lambda_3$ | $-23\times10^{-5}$ |
| Thermal expansion coefficients $\left(K^{-1}\right)$ | $\alpha_1 = \alpha_2$ | $12.3\times10^{-6}$ |
| | $\alpha_3$ | $8.2\times10^{-6}$ |
| Moisture expansion coefficients $\left(m^3k^{-1}\right)$ | $\beta_1$ | 0 |
| | $\beta_2 = \beta_3$ | $1.1\times10^{-4}$ |
| Density $\left(kg/m^3\right)$ | $\rho_f$ | 5500 |

Two face sheets are made up of a combination of piezoelectric and piezomagnetic materials. The main constituents of the face sheet are Barium Titanate $(BaTiO_3)$ and Cobalt Ferric oxide $(CoFe_2O_4)$. In this study, the volume fraction of $BaTiO_3 - CoFe_2O_4$ in each face sheet is chosen to be 0.5 and the material properties of magneto-electro-elastic face sheet are given in Table 1 [3].

### B. Material prorerties of FGM core layer

The FGM core layer is considered a mixture of ceramic and metal. According to the Voigt model, the property of functionally graded material may be expressed as

$$P = P_c V_c + P_m V_m. \tag{1}$$

where $P_c$ and $P_m$ are the corresponding properties of the ceramic and metal constituents, respectively. Here, $V_c$ and $V_m$ are the volume fractions of ceramic and metal that may be considered by power law distribution as [6]

$$V_c(z) = \left(\frac{2z+h}{2h}\right)^N, \quad V_m(z) = 1 - V_c(z). \tag{2}$$

where $N$ is the volume fraction exponent. Thus, the property of functionally graded material, such as Young's modulus, the thermal conductivity, and the coefficient of thermal expansion, vary as a power form of the thickness coordinate [6]

$$P_{eff}(z) = \mathrm{Pr}_c V_c(z) + \mathrm{Pr}_m V_m(z) \tag{3}$$

Because of the weak variation of Poisson's ratio in the constituent materials, it is considered constant in this paper. The smart sandwich plate is assumed to rest on Pasternak-type elastic foundations. The interaction between elastic foundations and the sandwich plate is defined as follows

$$q_e = k_1 w - k_2 \nabla^2 w. \tag{4}$$

where $\nabla^2 = \dfrac{\partial^2}{\partial x^2} + \dfrac{\partial^2}{\partial y^2}$, $w$ is the deflection of the smart sandwich plate, $k_1$ and $k_2$ are Winkler foundation stiffness and shear layer stiffness of Pasternak foundation, respectively.

### C. Boundary condition

In this study, depending on the in-plane restraint at the edges, four edges of the plate are simply supported and immovable. The associated boundary conditions are

$$\begin{aligned} &w = u = M_x = 0, N_x = N_{x0}, x = 0, a \\ &w = v = M_y = 0, N_y = N_{y0}, y = 0, b \end{aligned} \tag{5}$$

with $N_{x0}, N_{y0}$ are pre-buckling compressive force resultant in direction $x$.

## III. FUNDAMENTAL FORMULATION

Establishing the basic equations means finding reciprocal relationships between stress, strain and displacement components. These relationships are expressed in the strain compatibility equations, the equilibrium equation and Hooke's law.

It is easy to see here, the plate is the sandwich structure with three layers, in which the middle layer (core layer) is of the properties of FGM material and the two outer layers are taking into account the coupling between elastic, electric and magnetic field. The factors of temperature also influence these two outer layers. Therefore, it is necessary to establish the stress, strain and displacement components in each layer first.

*A. FGM core layer*

In this study, the classical plate theory is used to establish the basic equations and investigate the nonlinear dynamic buckling of the smart sandwich plate. The normal and shear strain components across the plate thickness at a distance $z$ from the mid-plane are defined as

$$\begin{Bmatrix} \varepsilon_x \\ \varepsilon_y \\ \gamma_{xy} \end{Bmatrix} = \begin{Bmatrix} \varepsilon_x^0 \\ \varepsilon_y^0 \\ \gamma_{xy}^0 \end{Bmatrix} + z\begin{Bmatrix} k_x \\ k_y \\ k_{xy} \end{Bmatrix} = \begin{Bmatrix} u_{,x} + 0.5w_{,x}^2 \\ v_{,y} + 0.5w_{,y}^2 \\ u_{,y} + v_{,x} + w_{,x}w_{,y} \end{Bmatrix} - z\begin{Bmatrix} w_{,xx} \\ w_{,yy} \\ 2w_{,xy} \end{Bmatrix} \quad (6)$$

where $\varepsilon_x^0, \varepsilon_y^0, \gamma_{xy}^0, \gamma_{xz}^0, \gamma_{yz}^0$ are the normal and transverse shear strains on the mid-plane of plate, and $u, v$ are displacement components along the $x, y$ directions of plate.

For FGM core layer, the relationship between stress and strain components with the effect of temperature are expressed as Hooke law is defined as

$$\begin{Bmatrix} \sigma_x \\ \sigma_y \\ \sigma_{xy} \end{Bmatrix}_a = \begin{bmatrix} Q_{11}^a & Q_{12}^a & 0 \\ Q_{12}^a & Q_{22}^a & 0 \\ 0 & 0 & Q_{66}^a \end{bmatrix} \begin{Bmatrix} \varepsilon_x \\ \varepsilon_y \\ \gamma_{xy} \end{Bmatrix}_a - \begin{Bmatrix} \alpha_1 \\ \alpha_2 \\ 0 \end{Bmatrix} \Delta T, \quad (7)$$

where $\Delta T$ is temperature rise from stress free initial state or temperature difference, and $E_a, \nu_a$ are elastic modulus and poisson's ratio of core layer,

$$Q_{11}^a = \frac{E_a}{1-\nu_a^2}, Q_{12}^a = \frac{\nu_a E_a}{1-\nu_a^2}, Q_{22}^a = Q_{11}^a, Q_{66}^a = \frac{E_a}{2(1+\nu_a)}.$$

*B. MEE face sheets*

The linear constitutive relations for magneto-electro-elastic face sheets taking into account the coupling between elastic, electric and magnetic fields can be represented as follows [1]

$$\begin{aligned}
\sigma_x^f &= \tilde{C}_{11}\varepsilon_x^f + \tilde{C}_{12}\varepsilon_y^f - \tilde{e}_{31}E_z - \tilde{q}_{31}H_z - \tilde{\alpha}_1\Delta T,\\
\sigma_y^f &= \tilde{C}_{12}\varepsilon_x^f + \tilde{C}_{22}\varepsilon_y^f - \tilde{e}_{32}E_z - \tilde{q}_{32}H_z - \tilde{\alpha}_2\Delta T,\\
\tau_{xy}^f &= \tilde{C}_{66}\gamma_{xy}^f,\\
D_x^f &= \tilde{\eta}_{11}E_x + \tilde{m}_{11}H_x + \tilde{p}_1\Delta T,\\
D_y^f &= \tilde{\eta}_{22}E_y + \tilde{m}_{22}H_y + \tilde{p}_2\Delta T,\\
D_z^f &= \tilde{e}_{31}\varepsilon_x + \tilde{e}_{32}\varepsilon_y + \tilde{\eta}_{33}E_z + \tilde{m}_{33}H_z + \tilde{p}_3\Delta T,\\
B_x^f &= \tilde{m}_{11}E_x + \tilde{\mu}_{11}H_x + \tilde{\lambda}_1\Delta T,\\
B_y^f &= \tilde{m}_{22}E_y + \tilde{\mu}_{22}H_y + \tilde{\lambda}_2\Delta T,\\
B_z^f &= \tilde{q}_{31}\varepsilon_x^f + \tilde{q}_{32}\varepsilon_y^f + \tilde{m}_{33}E_z + \tilde{\mu}_{33}H_z + \tilde{\lambda}_3\Delta T,
\end{aligned} \quad (8)$$

in which notation "$f$" represents for magneto-electro-elastic face sheets; $\sigma_x^f, \sigma_y^f, \tau_{xy}^f$, $D_i^f\ (i=x,y,z)$, and $B_i^f\ (i=x,y,z)$ are stress components, electric displacement and the magnetic flux respectively; $C_{ij}\ (ij=11,12,22,66)$, $e_{kl}(kl=31,32)$ and $q_{kl}(kl=31,32)$ are elastic coefficient, the piezoelectric coefficient and the magnetostrictive coefficient, respectively; $\alpha_i(i=1,2)$ and $\beta_i(i=1,2)$ are thermal expansion coefficients and moisture expansion coefficient, respectively. Further, $\eta_{ij}, m_{ij}$ and $\mu_{ij}$ with $(ij=11,22,33)$ are the dielectric constant, electromagnetic coefficient and the magnetic permeability constant, respectively; $p_i, \chi_i, \lambda_i\ (i=1,2,3)$ are the pyroelectric, hygroelectric, pyromagnetic and hygromagnetic material properties, respectively; $E_i$ and $H_i(x,y,z)$ are respectively electric field and magnetic field, and the reduced form of the parameters appearing in Eq. (8) can be clearly presented in Appendix.

The components of electric and magnetic fields $E_i$ and $H_i$ can be expressed by gradients of the scalar electric and magnetic potentials $\Phi$ and $\Psi$ as [11]

$$\{E_i, H_i\} = \{-\tilde{\Phi}_{,i}, -\tilde{\Psi}_{,i}\}, i = x, y, z. \quad (9)$$

in which the electric potential and magnetic potentials are assumed to have the form of combination of a cosine and linear function as follows

$$\begin{aligned}
\tilde{\Phi}(x,y,z,t) &= -\cos(\beta z)\Phi(x,y,t) + 2z\phi_0/h_f,\\
\tilde{\Psi}(x,y,z,t) &= -\cos(\beta z)\Psi(x,y,t) + 2z\psi_0/h_f,
\end{aligned} \quad (10)$$

where $\beta = \pi/h$, $\Phi(x,t), \Psi(x,t)$ are the spatial variation of the electric and magnetic potentials, respectively. Also, $\phi_0$ and $\psi_0$ are the initial external electric and magnetic potentials, respectively.

Substituting Eq. (10) into Eq. (9) yields

$$\begin{aligned}
&E_i = \cos(\beta z)(\Phi_{,i}), H_i = \cos(\beta z)(\Psi_{,i}), i = x, y \\
&E_z = -\beta\sin(\beta z)\Phi - 2\phi_0/h_f, H_z = -\beta\sin(\beta z)\Psi - 2\psi_0/h_f.
\end{aligned} \quad (11)$$

*C. The nonlinear motion and the deformation compatibility equation*

With the stress, strain and displacement components calculated for each of the material layers above, the force and moment resultants of the smart magneto-electro-elastic sandwich plate are expressed as

$$\begin{aligned}
(N_i, M_i) = &\int_{-h_2/2-h_3}^{-h_2/2} \sigma_i^f(1,z)dz + \int_{-h_2/2}^{0} \sigma_i^C(1,z)dz\\
&+ \int_{0}^{h_2/2} \sigma_i^C(1,z)dz + \int_{h_2/2}^{h_2/2+h_1} \sigma_i^f(1,z)dz, \ (i = x, y, xy)
\end{aligned} \quad (12)$$

Replacing Eq. (6) into Eqs. (7) and (8) then the results into Eq. (12) leads to

$$\begin{aligned}
N_x &= F_{11}\varepsilon_x^0 + F_{12}\varepsilon_y^0 + G_{11}k_x + G_{12}k_y - F_{13}E_z - G_{13}H_z - \alpha_1\Delta T,\\
N_y &= F_{12}\varepsilon_x^0 + F_{22}\varepsilon_y^0 + G_{12}k_x + G_{22}k_y - F_{14}E_z - G_{14}H_z - \alpha_2\Delta T,\\
N_{xy} &= F_{66}\gamma_{xy}^0 + G_{66}k_{xy},\\
M_x &= G_{11}\varepsilon_x^0 + G_{12}\varepsilon_y^0 + H_{11}k_x + H_{12}k_y - F_{23}E_z - G_{23}H_z - \alpha_3\Delta T,\\
M_y &= G_{12}\varepsilon_x^0 + G_{22}\varepsilon_y^0 + H_{12}k_x + H_{22}k_y - F_{24}E_z - G_{24}H_z - \alpha_4\Delta T\\
M_{xy} &= G_{66}\gamma_{xy}^0 + H_{66}k_{xy},
\end{aligned} \quad (13)$$

in which the detail of coefficients $A_{ij}\left(i=\overline{1,2}; j=\overline{1,4}\right)$, $A_{66}\ (A=F,G), H_{ij}(ij=11,12,22,66)$, $(\alpha,\beta)_i\left(i=\overline{1,4}\right)$ may be found in Appendix.

The nonlinear equilibrium equations of the sandwich plate using the Hamilton principle and the Volmir's

assumption with $u \ll w, v \ll w, \rho_1 u_{,tt} \to 0, \rho_1 v_{,tt} \to 0$ are defined as [18]

$$N_{x,x} + N_{xy,y} = 0, \tag{14a}$$

$$N_{xy,x} + N_{y,y} = 0, \tag{14b}$$

$$M_{x,xx} + 2M_{xy,xy} + M_{y,yy} + N_x w_{,xx} + 2N_{xy} w_{,xy} + N_y w_{,yy} + p - k_1 w + k_2 (w_{,xx} + w_{,yy}) = \rho_1 w_{,tt}. \tag{14c}$$

$$\int_{-h_c/2-h_f}^{-h_c/2} \left( \frac{\partial D_x}{\partial x}\cos(\beta z) + \frac{\partial D_y}{\partial y}\cos(\beta z) + D_z \beta \sin(\beta z) \right) dz + \int_{h_c/2}^{h_c/2+h_f} \left( \frac{\partial D_x}{\partial x}\cos(\beta z) + \frac{\partial D_y}{\partial y}\cos(\beta z) + D_z \beta \sin(\beta z) \right) dz = 0 \tag{14d}$$

$$\int_{-h_c/2-h_f}^{-h_c/2} \left( \frac{\partial B_x}{\partial x}\cos(\beta z) + \frac{\partial B_y}{\partial y}\cos(\beta z) + B_z \beta \sin(\beta z) \right) dz + \int_{h_c/2}^{h_c/2+h_f} \left( \frac{\partial B_x}{\partial x}\cos(\beta z) + \frac{\partial B_y}{\partial y}\cos(\beta z) + B_z \beta \sin(\beta z) \right) dz = 0 \tag{14e}$$

in which, $p(Pa)$ is an external pressure uniformly distributed on the surface of the sandwich plate and

$$\rho_1 = \int_{-hf-hc/2}^{-hc/2} \rho_f(z)dz + \int_{-hc/2}^{hc/2} \rho_c(z)dz + \int_{hc/2}^{hc/2+hf} \rho_f(z)dz.$$

The deformation compatibility equation for a sandwich plate can be written as

$$\varepsilon^0_{x,yy} + \varepsilon^0_{y,xx} - \gamma^0_{xy,xy} = (w_{,xy})^2 - w_{,xx} w_{,yy} + 2w_{,xy} w^*_{,xy} - w_{,xx} w^*_{,yy} - w_{,yy} w^*_{,xx}. \tag{15}$$

in which $w^*(x,y)$ is function of initial imperfection.

## IV. SOLUTIONS TO THE PROBLEM

Base on the classical plate theory, the stress function method is applied to solve the problem, in which the chosen stress function Airy is introduced as

$$N_x = f_{,yy}, N_y = f_{,xx}, N_{xy} = -f_{,xy}. \tag{16}$$

Replace this stress function into Eqs. (14) and (15), while performing the necessary transformations, it can be seen that the four newly obtained equations are two nonlinear equations in terms of variables $w, f, \Phi$ and $\Psi$ used to investigate the nonlinear vibration and dynamic of MEE-FGM-MEE sandwich plate surrounded on elastic foundations.

To solve four newly equations above and with the consideration of the boundary conditions (5), we assume the following approximate solutions:

$$\begin{aligned} w(x,y,t) &= W(t)\sin\lambda_m x \sin\delta_n y, \\ \Phi(x,y,t) &= \phi(t)\sin\lambda_m x \sin\delta_n y, \\ \Psi(x,y,t) &= \psi(t)\sin\lambda_m x \sin\delta_n y, \\ w^*(x,y,t) &= \mu h \sin\lambda_m x \sin\delta_n y, \\ f(x,y,t) &= A_1\cos 2\lambda_m x + A_2 \cos 2\delta_n y + \\ &+ A_3 \sin\lambda_m x \sin\delta_n y + 0.5N_{x0}y^2 + 0.5N_{y0}x^2 \end{aligned} \tag{17}$$

where $\lambda_m = m\pi/a$ , $\delta_n = n\pi/b$ , $W$ is the amplitude of the deflection and $m, n$ are odd natural numbers; $\phi$ and $\psi$ are electric and magnetic potentials, respectively. The coefficients $A_i$ $(i = 1 \div 3)$ are determined by substitution of Eq. (17) into the deformation compatibility equation, and:

$$A_1 = M_1 W(W + 2\mu h),\ A_2 = M_2 W(W + 2\mu h),\ A_3 = M_3 W,$$

$$M_1 = \delta_n^2 / 32F^*_{11}\lambda_m^2,\ M_2 = \lambda_m^2 / 32F^*_{22}\delta_n^2,$$

$$M_3 = -\frac{\left[G^*_{21}\lambda_m^4 + \left(G^*_{11} + G^*_{22} - 2G^*_{66}\right)\lambda_m^2\delta_n^2 + G^*_{12}\delta_n^4\right]}{\left[F^*_{11}\lambda_m^4 - \left(2F^*_{12} - F^*_{66}\right)\lambda_m^2\delta_n^2 + F^*_{22}\delta_n^4\right]}$$

Substitution of the approximate solutions (17) into the nonlinear motion equations and applying the Galerkin procedure for resulting equation yield

$$\begin{aligned} &h_{11}W + h_{12}W(W + \mu h) + h_{13}W(W + 2\mu h) + \\ &+ h_{14}W(W + \mu h)(W + 2\mu h) + h_{15}\phi + h_{16}\psi + \\ &- \left(N_{x0}\lambda_m^2 + N_{y0}\delta_m^2\right)(W + \mu h) + n_5 p = \rho_1 W_{,tt}, \\ &h_{41}W + h_{42}\phi + h_{43}\psi = 0, \\ &h_{51}W + h_{43}\phi + h_{52}\psi = 0. \end{aligned} \tag{18}$$

where $h_{ij}\,(i = 1, j = 1 \div 6), h_{4l}\,(l = 1 \div 3), h_{51}, h_{52}, n_5$ are shown in Appendix.

The conditions expressing the immovability on four edges (i.e. $u = 0$ on $x = 0, a$ and $v = 0$ on $y = 0, b$ ) are satisfied on the average sense as

$$\int_0^b \int_0^a \frac{\partial u}{\partial x}dxdy = 0,\ \int_0^a \int_0^b \frac{\partial v}{\partial x}dydx = 0. \tag{19}$$

in which, the formulas of the normal and shear strains in the middle surface of the sandwich plate can be determine from Eq. (13) as

$$\begin{aligned} \varepsilon^0_x &= F^*_{22}f_{,yy} - F^*_{12}f_{,xx} + G^*_{11}w_{,xx} + G^*_{12}w_{,yy} + F^*_{13}\phi_0 + G^*_{13}\psi_0 + \alpha^*_1\Delta T, \\ \varepsilon^0_y &= F^*_{11}f_{,xx} - F^*_{12}f_{,yy} + G^*_{21}w_{,xx} + G^*_{22}w_{,yy} + \\ &+ F^*_{14}\phi_0 + G^*_{14}\psi_0 + \alpha^*_2\Delta T, \\ \gamma^0_{xy} &= -F^*_{66}f_{,xy} + 2G^*_{66}w_{,xy}, \end{aligned} \tag{20}$$

with: $\alpha^*_1 = F^*_{22}\alpha_1 - F^*_{12}\alpha_2, \alpha^*_2 = F^*_{11}\alpha_2 - F^*_{12}\alpha_1, F^*_{11} = F_{11}/\Delta,$

$F^*_{22} = F_{22}/\Delta, F^*_{12} = F_{12}/\Delta, F^*_{66} = 1/F_{66}, G^*_{66} = G_{66}/F_{66},$

$\Delta = F_{11}F_{22} - F_{12}^2, G^*_{11} = F^*_{22}G_{11} - F^*_{12}G_{12}, G^*_{22} = F^*_{11}G_{22} - F^*_{12}G_{12}$

$G^*_{12} = F^*_{22}G_{12} - F^*_{12}G_{22}, G^*_{21} = F^*_{11}G_{12} - F^*_{12}G_{11},$

$F^*_{13} = -2\left(F^*_{22}F_{13} - F^*_{12}F_{14}\right)/h_f, G^*_{13} = -2\left(F^*_{22}G_{13} - F^*_{12}G_{14}\right)/h$

$F^*_{14} = -2\left(F^*_{11}F_{14} - F^*_{12}F_{13}\right)/h_f, G^*_{14} = -2\left(F^*_{11}G_{14} - F^*_{12}G_{13}\right)/h$

From Eqs. (6) and (20), the derivative of displacement in the $x$ and $y$ directions are determined as

$$\begin{aligned} v_{,y} &= F^*_{11}f_{,xx} - F^*_{12}f_{,yy} + G^*_{21}w_{,xx} + G^*_{22}w_{,yy} + \\ &+ F^*_{14}\phi_0 + G^*_{14}\psi_0 + \alpha^*_2\Delta T - \left(w_{,y}\right)^2/2 - w_{,y}w^*_{,y}, \\ u_{,x} &= F^*_{22}f_{,yy} - F^*_{12}f_{,xx} + G^*_{11}w_{,xx} + G^*_{12}w_{,yy} + \\ &+ F^*_{13}\phi_0 + G^*_{13}\psi_0 + \alpha^*_1\Delta T - \left(w_{,x}\right)^2/2 - w_{,x}w^*_{,x}, \end{aligned}$$

Introducing Eq (17) into Eq. (21) then obtained re into Eq. (19) leads to

$$N_{x0} = g_1 W + g_2(W + 2\mu h)W + g_3\phi_0 + g_4\psi_0 + g_5\Delta T,$$
$$N_{y0} = f_1 W + f_2(W + 2\mu h)W + f_3\phi_0 + f_4\psi_0 + f_5\Delta T, \quad (22)$$

here $g_i, f_j\,(i, j = 1 \div 5)$ are shown in Appendix.

It is assumed that uniformly distributed transverse load has the form of $p = st$, the equations are used to study the nonlinear vibration of sandwich plate in the thermal environment is written as

$$W_{,tt} + o_{11}W + o_{11}^{*}(W + \mu h) + o_{12}W(W + \mu h) + o_{15}\phi + o_{16}\psi$$
$$+ o_{13}^{*}(W + \mu h)(W + 2\mu h) + + o_{14}W(W + \mu h)(W + 2\mu h)$$
$$+ o_{13}W(W + 2\mu h) + o_{15}^{*}\phi(W + \mu h) + o_{16}^{*}\psi(W + \mu h) = n_5 st, \quad (23)$$
$$h_{41}W + h_{42}\phi + h_{43}\psi = 0,$$
$$h_{51}W + h_{43}\phi + h_{52}\psi = 0.$$

where the $o_{1i}\,(i = 1 \div 6), o_{1j}^{*}\,(j = 1,3)$ - coefficients, as shown in Appendix.

The fundamental frequency of natural vibration of the sandwich plate can be determined by finding the solution of under equation

$$\begin{vmatrix} o_{11} + o_{11}^{*} - \omega^2 & o_{15} & o_{16} \\ h_{41} & h_{42} & h_{43} \\ h_{51} & h_{43} & h_{52} \end{vmatrix} = 0 \quad (24)$$

To determine the value of the dynamic critical load, this study uses the the Budiansky–Roth criterion [17], with the time of instability as the time when the deflection amplitude - time curve reaches its maximum value first.

## V. RESULTS AND DISCUSSION

### A. Comparison results

In order to ensure the accuracy of present approach, the values of the dimensionless frequencies and fundamental frequencies of the FGM plate are calculated and compared with the results obtained by the other authors, such as Bich [14, 18], Alijani [15] and Kim [16]. The comparison results are shown in Tables 2, 3 with the following characteristic parameters: $\rho_m = 2702\,kg/m^3$, $\rho_c = 3800\,kg/m^3$ and $E_c = 380\times10^9\,N/m^2$.

TABLE II. COMPARISON OF DIMENSIONLESS FREQUENCIES $\Omega = \omega_L a/\sqrt{c_{\max}/\rho_{\max}}$ OF FGM PLATE WITH $a/b = 1, a/h = 0.1$,

| $N$ | Present study | Bich [14] | Alijani [15] | Kim [16] |
|---|---|---|---|---|
| 0 | 0.0581 | 0.0597 | 0.0579 | 0.0582 |
| 0.5 | 0.0505 | 0.0506 | 0.0506 | 0.0532 |
| 1 | 0.0447 | 0.0456 | 0.0456 | 0.0437 |
| 4 | 0.0389 | 0.0396 | 0.0396 | 0.0393 |
| 10 | 0.0363 | 0.0381 | 0.0380 | 0.0359 |

here $c_{\max}$, $\rho_{\max}$ are the maximum values of elastic constants and mass densities of piezoelectric and magnetostrictive layers, respectively.

TABLE III. COMPARISON OF FUNDAMENTAL FREQUENCIES OF NATURAL VIBRATION $(rad/s)$ OF FGM PLATE WITH $a = b = 1.5, h = 0.008$.

| N | 0.2 | 1 | 5 | 10 |
|---|---|---|---|---|
| Present study | 197.114 | 162.112 | 139.794 | 135.384 |
| Bich [18] | 197.110 | 162.110 | 139.790 | 135.380 |

As can be seen, with the change of the volume fraction exponent $N$, the difference between the results shown in the table is not too large, or in other words, the present results agree very well with existing predictions, which indicates the reliability of present study.

### B. Dynamic critical load

In this part, the influence of the parameters on the dynamic critical load value will be investigated.

Table 4 shows the effect of elastic foundations with two coefficients $k_1(GPa/m)$, $k_2(GPa.m)$, modes of vibration $(m,n)$ and the loading speed $s$ on the dynamic critical load value of sandwich MEE-FGM-MEE plate with rectangular cross-section $a/b = 1$.

TABLE IV. EFFECTS OF ELASTIC FOUNDATIONS, MODES OF VIBRATION AND THE LOAD SETTING SPEED ON THE DYNAMIC CRITICAL LOAD VALUE

| | | $(m,n)$ | | |
|---|---|---|---|---|
| $(k_1,k_2)$ | $s$ | (1,1) | (1,2) | (1,3) |
| | 3.5e11 | 8.1472e+7 | 8.9162e+7 | 9.7842e+7 |
| *(0,0)* | 5e11 | 11.6389e+7 | 12.7374e+7 | 13.9748e+7 |
| | 7.5e11 | 17.4584e+7 | 19.1062e+7 | 20.9623e+7 |
| | 3.5e11 | 8.1886e+7 | 8.9183e+7 | 9.7963e+7 |
| *(0.1e9,0)* | 5e11 | 11.6980e+7 | 12.7405e+7 | 13.9947e+7 |
| | 7.5e11 | 17.5470e+7 | 19.1107e+7 | 20.9921e+7 |
| | 3.5e11 | 8.2589e+7 | 10.9986e+7 | 12.0764e+7 |
| *(0.1e9, 0.02e9)* | 5e11 | 11.7985e+7 | 15.6980e+7 | 17.2520e+7 |
| | 7.5e11 | 17.6977e+7 | 23.5470e+7 | 25.8780e+7 |

As can be observed, the value of the dynamic critical load of the sandwich plate with the support of elastic foundations is higher than one of sandwich plate without elastic foundations. The elastic foundations enhance the stiffness of the sandwich plate. Further, the value of the dynamic critical load increases significantly when the values of modes $(m,n)$ and the loading speed $s$ increase and vice versa with $(m,n), s$ decrease.

TABLE V. EFFECTS OF TEMPERATURE INCREMENT, THE RATIO $b/h$ AND THE MAGNETIC POTENTIAL $\phi_0$ ON THE DYNAMIC CRITICAL LOAD VALUE

| $\Delta T(K)$ | $b/h$ | $\phi_0$ | | |
|---|---|---|---|---|
| | | -100 | 0 | 100 |
| | 80 | 1.064876e+8 | 1.064873e+8 | 1.0648725e+8 |
| 0 | 90 | 1.133963e+8 | 1.1339613e+8 | 1.133960e+8 |
| | 100 | 1.206422e+8 | 1.2064035e+8 | 1.2064032e+8 |
| | 80 | 1.06594e+8 | 1.06592e+8 | 1.065918e+8 |
| 100 | 90 | 1.134433e+8 | 1.134417e+8 | 1.134418e+8 |
| | 100 | 1.207651e+8 | 1.207647e+8 | 1.207646e+8 |
| | 80 | 1.094731e+8 | 1.094725e+8 | 1.094713e+8 |
| 200 | 90 | 1.135035e+8 | 1.135032e+8 | 1.1350315e+8 |
| | 100 | 1.20921e+8 | 1.209197e+8 | 1.209195e+8 |

The effects of temperature increment $\Delta T$, the plate width to thickness ratio $b/h$ and magnetic potential $\phi_0$ on the dynamic critical load value of the sandwich plate with rectangular cross-section $a/b = 1$ resting on elastic foundation are given in Table 5. As expected, the increase of temperature increment $\Delta T$, increase of ratio $b/h$ and

decrease of the magnetic potential value results in the increase of the dynamic critical load value. However, the difference of the dynamic critical load is not significant with the change of all three values examined.

TABLE VI. EFFECTS OF VOLUME FRACTION EXPONENT, THE RATIO $a/b$ AND THE MAGNETIC POTENTIAL $\psi_0$ ON THE DYNAMIC CRITICAL LOAD VALUE OF SANDWICH PLATE

| $N$ | $a/b$ | $\psi_0$ | | |
|---|---|---|---|---|
| | | -200 | 0 | 200 |
| 0 | 0.5 | 7.51634e+7 | 7.51674e+7 | 7.51679e+7 |
| | 1 | 9.74085e+7 | 9.74157e+7 | 9.741621e+7 |
| | 1.5 | 10.45975e+7 | 10.46078e+7 | 10.46083e+7 |
| 1 | 0.5 | 8.26773e+7 | 8.26787e+7 | 8.267905e+7 |
| | 1 | 10.6592e+7 | 10.6594e+7 | 10.6596e+7 |
| | 1.5 | 11.36364e+7 | 11.36368e+7 | 11.36373e+7 |
| 2 | 0.5 | 8.49963e+7 | 8.49977e+7 | 8.49991e+7 |
| | 1 | 11.27222e+7 | 11.27276e+7 | 11.27331e+7 |
| | 1.5 | 11.93382e+7 | 11.93387e+7 | 11.93392e+7 |

The influences of volume fraction exponent $N$, ratio $a/b$ and magnetic potentials $\psi_0$ $(A)$ on the dynamic critical load value of the sandwich plate resting on elastic foundation are presented in Table 8. It is found that the effects of electric potentials are very small, the dynamic critical load value decreases as the electric potential decreases. Also, the ratio $a/b$ and the volume fraction exponent have significant effect on the dynamic critical load of the smart sandwich plate. The value of the dynamic critical load increases significantly when the values of ratio $a/b$ and the volume fraction exponent $N$ increase.

*C. The deflection amplitude - time curve*

The influence of the parameters on the nonlinear dynamic response of sandwich plate will be investigated in this part.

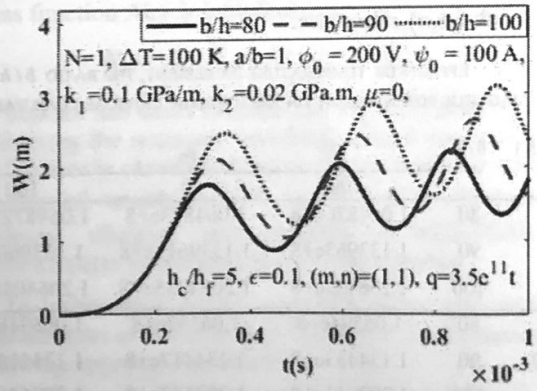


Fig. 2. Effects of initial imperfection on the nonlinear dynamic response of the sandwich plate.

Fig. 2 indicates the effects of length to thickness $b/h$ on nonlinear dynamic response of the sandwich plate. As seen, an increase of ratios $b/h$ results in a rise of the deflection amplitude of the sandwich plate.

The influences of the volume fraction exponent $N$ and initial imperfection $\mu$ on the nonlinear dynamic response of the sandwich plate is given in Fig. 3 and Fig. 4. As can be seen, similar to the effect on the dynamic critical load value, the volume fraction exponent has very significantly effect on the deflection amplitude of the sandwich plate, while the imperfection has slightly effect.

Fig. 5 indicates the effects of temperature increment on the nonlinear dynamic response of the sandwich plate. Same as the results shown in Table 5, $\Delta T$ has very small effect on the deflection amplitude of the sandwich plate. An increase of temperature increment which is external impact reduce the stiffness of the sandwich plate results in a rise of the deflection amplitude of the smart sandwich plate.

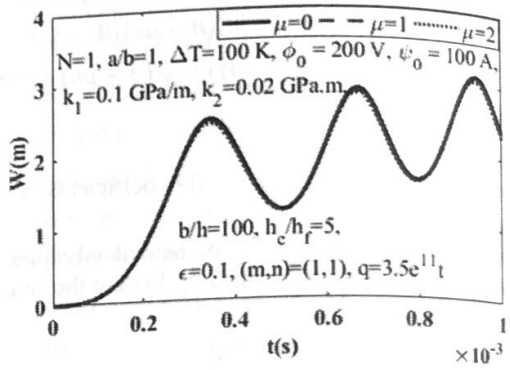


Fig. 3. Effects of ratio $b/h$ on the nonlinear dynamic response of the sandwich plate.

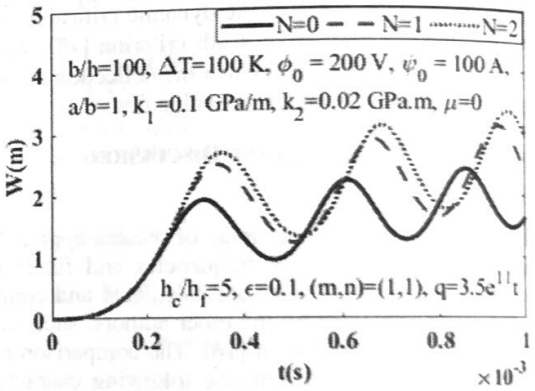


Fig. 4. Effects of volume fraction exponent on the nonlinear dynamic response of the sandwich plate.

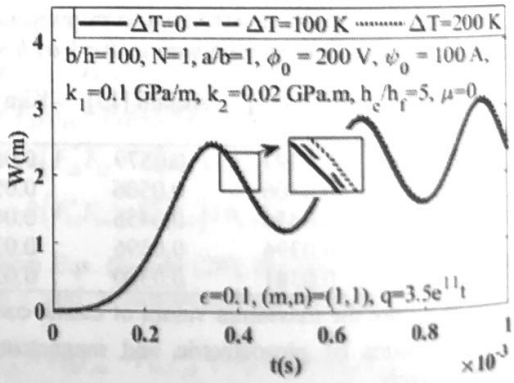


Fig. 5. Effects of temperature increment $\Delta T$ on the nonlinear dynamic response of the sandwich plate.

Figs. 6 and 7 illustrate the effect of elastic foundation on the nonlinear dynamic response of the sandwich plate, respectively. As can be seen, the deflection amplitude will become lower as two coefficients $k_1$ and $k_2$ increase. In other words, the elastic foundations increase the stiffness of

the sandwich plate and the elastic modulus of the sandwich plate are increased due to the support of elastic foundations. Results from Figs. 6 and 7 also indicate that the effect of Pasternak foundation is more prominent than one of Winkler foundation.

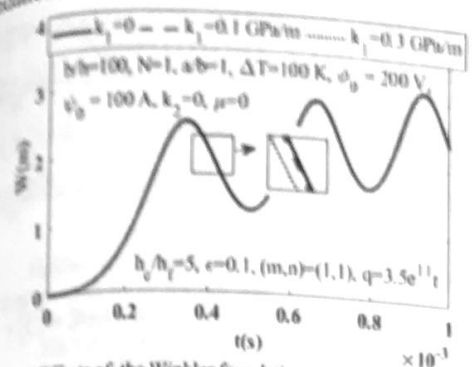


Fig. 6. Effects of the Winkler foundation stiffness on the nonlinear dynamic response of the sandwich plate.

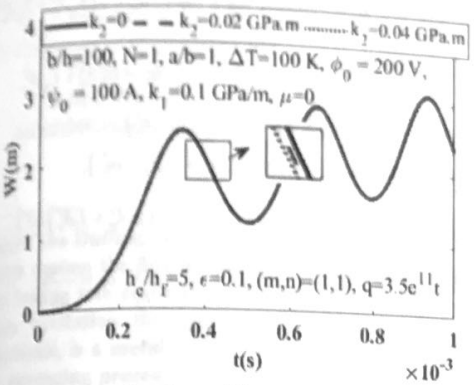


Fig. 7. Effects of the shear layer stiffness of Pasternak foundation on the nonlinear dynamic response of the sandwich plate.

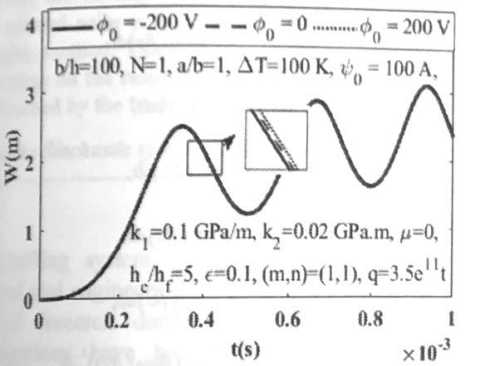


Fig. 8. Effects of electric potential on the nonlinear dynamic response of the sandwich plate.

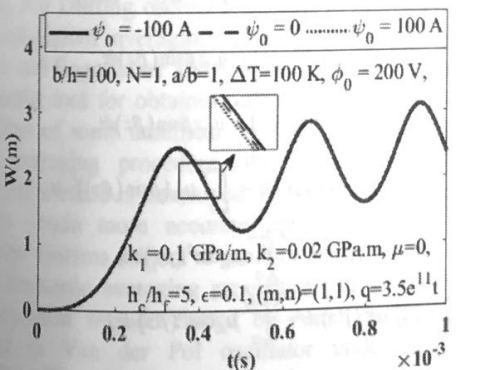


Fig. 9. Effects of magnetic potential on the nonlinear dynamic response of the sandwich plate.

The influences of magnetic and electric potentials on the deflection amplitude - time curve of the sandwich plate are depicted in Figs. 8 and 9, respectively. It is observed that both of electric and magnetic potentials have small effect on the nonlinear dynamic response of sandwich plate. The deflection amplitude of the sandwich plate with higher electric potential is higher than one with lower electric potential, whereas it becomes lower when the magnetic potential increases.

## VI. Conclusions

By using an analytical method based on classical plate theory, the nonlinear dynamic buckling of the sandwich plate with two MEE face sheets and FGM core layer subjected to the combination of external pressure, thermal, electric, and magnetic loads were elucidated in this paper. In addition to surveys on the influence of geometrical and material parameters, a point worth noting here is by evaluating the influence of electric and magnetic potentials – the typical parameters of the MEE layer, it can be concluded that although both of them are considered to be external forces, they have small effect on the dynamic critical load of the sandwich plate with FGM core layer. In other words, the addition of MEE layers has little effect on the nonlinear dynamic buckling of sandwich plate with FGM core layer in the thermal environment, while they complement the plate with the advantages of magnetism and electrical properties, thereby expanding the scope of applications of FGM structures in sensors, civil structures, aerospace control systems and medical devices…

## References

[1] M. Vinyas, "Computational Analysis of Smart Magneto – Electro – Elastic Materials and Structures: Review and Classifcation', Archives of Computational Methods in Engineering, 2020.

[2] B. Saleh, J. Jiang, A. Ma, D. Song, D. Yang, "Effect of main parameters on the mechanical and wear behaviour of functionally graded materials by centrifugal casting: a review". Met Mater Int., https://doi.org/10.1007/s12540-019-00273-8, 2019.

[3] M. Vinyas, S.C. Kattimani, "Static studies of stepped functionally graded magneto-electro-elastic beam subjected to different thermal loads", Compos. Struct 163, 216– 237, 2017.

[4] P. Zhang, C. Qi, H. Fang, C. Ma, Y. Huang, "Semi-analytical analysis of static and dynamic responses for laminated magneto-electro-elastic plates", Compos. Struct. 110933, 2019.

[5] M.C. Kiran, S.C. Kattimani, "Free Vibration of Multilayered Magneto-Electro-Elastic Plates With Skewed Edges Using Layer wise Shear Deformation Theory", Materials Today: Proceedings, 5(10), 21248–21255, 2018.

[6] N.D Duc, D.H Bich, V.T.T. Anh, "On the nonlinear stability of eccentrically stiffened functionally graded annular spherical segment shells", J. Thin-Walled Structures. Vol. 106, pp. 258-267, 2016.

[7] P.V. Vinh, N.T. Dung, N.C. Tho, D.V. Thom, L.K. Hoa, "Modified single variable shear deformation plate theory for free vibration analysis of rectangular FGM plates", Structures, 29, 1435-1444, 2021.

[8] D.H. Bich, D.G. Ninh. T.I. Thinh, "Nonlinear buckling analysis of FGM toroidal shell segments filled inside by an elastic medium under external pressure loads including temperature effects", Composites Part B: Engineering, 87, 75-91, 2016.

[9] V.H. Nam, N.T. Phuong, K.V. Minh, P.T. Hieu, "Nonlinear thermo-mechanical buckling and post-buckling of multilayer FGM cylindrical shell reinforced by spiral stiffeners surrounded by elastic foundation subjected to torsional loads". European Journal of Mechanics - A/Solids, 72, 393-406, 2018.

[10] M. Arefi, A.M. Zenkour, "Thermo-electro-magneto-mechanical bending behavior of size-dependent sandwich piezomagnetic nanoplates", Mechanics Research Communications, 84, 27–42, 2017.

[11] N.D. Dat, T.Q. Quan, V. Mahesh, N.D. Duc, "Analytical solutions for nonlinear magneto-electro-elastic vibration of smart sandwich plate

with carbon nanotube reinforced nanocomposite core in hygrothermal environment". Inter. J. of Mechan. Scien., 105906, 2020.

[12] D. Xiao, Q. Han, T. Jiang, "Guided wave propagation in a multilayered magneto-electro-elastic curved panel by Chebyshev spectral elements method" Compos. Struct. , 207, 701-710, 2019.

[13] V.T.T Anh, P.N. Thinh, V.D. Quang, N.D. Duc, "Impact of blast and mechanical loads on the shear deformable stiffened sandwich plate with an auxetic core layer in thermal environment", *J. Sandwich Struct. and Materials*, 0(0) 1–33, 2021.

[14] D.H. Bich, D.V. Dung, V.H. Nam, Nonlinear dynamical analysis of eccentrically stiffened functionally graded cylindrical panels, Compos. Struct. 94, 2465–2473, 2012.

[15] F. Alijani, M. Amabili, K. Karagiozis, F. Bakhtiari-Nejad, Nonlinear vibrations of functionally graded doubly curved shallow shells, J. Sound Vib. 330 (2011) 1432–1454.

[16] S.E. Kim, N.D. Duc, V.H. Nam, N.V. Sy, "Nonlinear vibration and dynamic buckling of eccentrically oblique stiffened FGM plates resting on elastic foundations in thermal environment", Thin-Walled Structures, 142, 287–296. doi:10.1016/j.tws.2019.05.013, 2019.

[17] B. Budiansky, and R. S. Roth, "Axisymmetric dynamic buckling of clamped shallow spherical shells", NASA technical note D_510, 1962, 597–609, 2012.

[18] D.H Bich, D.V Dung, V.H Nam, "Nonlinear dynamical analysis of eccentrically stiffened functionally graded cylindrical panels", 94(8), 2465-2473, 2012.

## APPENDIX

$$(F_{ij}, G_{ij}, H_{ij}) = \int_{-h_f-h_c/2}^{-h_c/2} \tilde{C}_{ij}(1, z, z^2)dz + \int_{-h_c/2}^{0} Q_{ij}(1, z, z^2)dz +$$
$$+ \int_{0}^{h_c/2} Q_{ij}(1, z, z^2)dz + \int_{h_c/2}^{h_c/2+h_f} \tilde{C}_{ij}(1, z, z^2)dz, \ (ij = 11,12,22,66),$$

$$(F_{13}, F_{23}) = \int_{-h_f-h_c/2}^{-h_c/2} \tilde{e}_{31}(1, z)dz + \int_{h_c/2}^{h_c/2+h_f} \tilde{e}_{31}(1, z)dz,$$

$$(F_{14}, F_{24}) = \int_{-h_f-h_c/2}^{-h_c/2} \tilde{q}_{31}(1, z)dz + \int_{h_c/2}^{h_c/2+h_f} \tilde{q}_{31}(1, z)dz,$$

$$(G_{13}, G_{23}) = \int_{-h_f-h_c/2}^{-h_c/2} \tilde{e}_{32}(1, z)dz + \int_{h_c/2}^{h_c/2+h_f} \tilde{e}_{32}(1, z, z^3)dz,$$

$$(G_{14}, G_{24}) = \int_{-h_f-h_c/2}^{-h_c/2} \tilde{q}_{32}(1, z)dz + \int_{h_c/2}^{h_c/2+h_f} \tilde{q}_{32}(1, z)dz,$$

$$\alpha_1 = \int_{-h_f-h_c/2}^{-h_c/2} (Q_{11} + Q_{12})\tilde{\alpha}_1(1, z)dz + \int_{-h_c/2}^{0} Q_{11}\alpha_{11}(1, z)dz + \int_{0}^{h_c/2} Q_{11}\alpha_{11}(1, z)dz$$
$$+ \int_{-h_c/2}^{0} Q_{12}\alpha_{22}(1, z)dz + \int_{0}^{h_c/2} Q_{12}\alpha_{22}(1, z)dz + \int_{h_c/2}^{h_f+h_c/2} (Q_{11} + Q_{12})\tilde{\alpha}_1(1, z)dz,$$

$$\alpha_2 = \int_{-h_f-h_c/2}^{-h_c/2} (Q_{12} + Q_{22})\tilde{\alpha}_2(1, z)dz + \int_{-h_c/2}^{0} Q_{12}\alpha_{11}(1, z)dz + \int_{0}^{h_c/2} Q_{12}\alpha_{11}(1, z)dz$$
$$+ \int_{-h_c/2}^{0} Q_{22}\alpha_{22}(1, z)dz + \int_{0}^{h_c/2} Q_{22}\alpha_{22}(1, z)dz + \int_{h_c/2}^{h_f+h_c/2} (Q_{12} + Q_{22})\tilde{\alpha}_2(1, z)dz,$$

$$\tilde{C}_{11} = C_{11} - \frac{C_{13}^2}{C_{33}}, \tilde{C}_{12} = C_{12} - \frac{C_{13}C_{23}}{C_{33}}, \tilde{C}_{22} = C_{22} - \frac{C_{23}^2}{C_{33}}, \tilde{C}_{66} = C_{66}, \ \tilde{\lambda}_1 = \lambda_1,$$

$$\tilde{\lambda}_2 = \lambda_2, \tilde{e}_{31} = e_{31} - C_{13}\frac{e_{33}}{C_{33}}, \tilde{e}_{32} = e_{32} - C_{23}\frac{e_{33}}{C_{33}}, \tilde{q}_{31} = q_{31} - \frac{C_{13}q_{33}}{C_{33}},$$

$$\tilde{q}_{32} = q_{32} - \frac{C_{13}q_{33}}{C_{33}}, \tilde{\mu}_{11} = \mu_{11} + \frac{q_{15}^2}{C_{55}}, \tilde{\mu}_{22} = \mu_{22} + \frac{q_{24}^2}{C_{44}}, \tilde{\mu}_{33} = \mu_{33} + \frac{q_{33}^2}{C_{33}},$$

$$\tilde{p}_2 = p_2, \ \tilde{\eta}_{11} = \eta_{11} + \frac{e_{15}^2}{C_{55}}, \ \tilde{\eta}_{22} = \eta_{22} + \frac{e_{24}^2}{C_{44}}, \tilde{\eta}_{33} = \eta_{33} + \frac{e_{33}^2}{C_{33}}, \ \tilde{p}_1 = p_1,$$

$$\tilde{m}_{33} = m_{33} + \frac{e_{33}q_{33}}{C_{33}}, \tilde{\alpha}_1 = \alpha_1 - \frac{C_{13}\alpha_3}{C_{33}}, \tilde{m}_{11} = m_{11} + \frac{e_{15}q_{15}}{C_{55}}, \tilde{m}_{22} = m_{22} + \frac{e_{24}q_{24}}{C_{44}},$$

$$\tilde{\alpha}_2 = \alpha_2 - \frac{C_{23}\alpha_3}{C_{33}}, \ \tilde{p}_3 = p_3 + \frac{e_{33}\alpha_{33}}{C_{33}}, \tilde{\lambda}_3 = \lambda_3 + \frac{q_{33}\alpha_{33}}{C_{33}}.$$

$$L_{11}^* = H_{11} - G_{11}^*G_{11} - G_{21}^*G_{12}, \ L_{22}^* = H_{22} - G_{12}^*G_{12} - G_{22}^*G_{22},$$
$$L_{12}^* = H_{12} - G_{12}^*G_{11} - G_{22}^*G_{12}, \ L_{21}^* = H_{12} - G_{11}^*G_{12} - G_{21}^*G_{22},$$
$$L_{66}^* = H_{66} - G_{66}^*G_{66}, L_{31}^* = (-F_{23})\beta\sin(\beta z), L_{32}^* = (-F_{24})\beta\sin(\beta z),$$
$$L_{41}^* = (-G_{23})\beta\sin(\beta z), L_{42}^* = (-G_{24})\beta\sin(\beta z),$$

$$g_1 = \frac{-4}{H^* ab\lambda_m\delta_n}\left[\left(F_{12}^*G_{11}^* + F_{22}^*G_{21}^*\right)\lambda_m^2 + \left(F_{11}^*G_{12}^* + F_{12}^*G_{22}^* + M_3\left(F_{11}^*F_{22}^* - F_{12}^{*2}\right)\right)\delta_n^2\right],$$
$$H^* = F_{12}^{*2} - F_{11}^*F_{22}^*, \ g_2 = -\frac{F_{11}^*\lambda_m^2 + F_{12}^*\delta_n^2}{8H^*}, g_3 = \frac{F_{11}^*F_{13}^* + F_{12}^*F_{14}^*}{H^*}, g_4 = \frac{F_{11}^*G_{13}^* + F_{12}^*G_{14}^*}{H^*},$$

$$f_1 = \frac{-4}{H^* ab\lambda_m\delta_n}\left[\left(F_{12}^*G_{11}^* + F_{22}^*G_{21}^* + M_3\left(F_{11}^*F_{22}^* - F_{12}^{*2}\right)\right)\lambda_m^2 + \left(F_{12}^*G_{12}^* + F_{22}^*G_{22}^*\right)\delta_n^2\right],$$
$$f_2 = -\frac{F_{12}^*\lambda_m^2 + F_{22}^*\delta_n^2}{8H^*}, f_3 = \frac{F_{12}^*F_{13}^* + F_{22}^*F_{14}^*}{H^*}, g_3 = \frac{F_{11}^*\alpha_1^* + F_{12}^*\alpha_2^*}{H^*}, f_4 = \frac{F_{12}^*G_{13}^* + F_{22}^*G_{14}^*}{H^*},$$
$$f_5 = \frac{F_{12}^*\alpha_1^* + F_{22}^*\alpha_2^*}{H^*}.$$

$$h_{11} = -\left[L_{11}^*\lambda_m^4 + L_{22}^*\delta_n^4 + \left(L_{12}^* + L_{21}^* + 4L_{66}^*\right)\lambda_m^2\delta_n^2 + k_1 + k_2\left(\lambda_m^2 + \delta_n^2\right)\right] +$$
$$+\left[G_{21}^*\lambda_m^4 + G_{12}^*\delta_n^4 + \left(G_{11}^* + G_{22}^* - 2G_{66}^*\right)\lambda_m^2\delta_n^2\right]M_3,$$
$$h_{12} = \frac{-32\lambda_m\delta_n M_3}{3ab}, \ h_{13} = -\frac{8\lambda_m\delta_n}{3ab}\left(\frac{G_{21}^*}{F_{11}^*} + \frac{G_{12}^*}{F_{22}^*}\right), \ h_{31} = -\left(T_{21}\lambda_m^2 + T_{22}\delta_n^2\right),$$

$$h_{14} = -\frac{\left(\lambda_m^4/F_{22}^* + \delta_n^4F_{11}^*\right)}{16}, \ h_{15} = L_{31}^*\lambda_m^2 + L_{32}^*\delta_n^2, \ h_{16} = L_{41}^*\lambda_m^2 + L_{42}^*\delta_n^2,$$
$$h_{32} = -\left(T_{23}\lambda_m^2 + T_{24}\delta_n^2 - \mu_{33}^*\right), \ h_{41} = -\left(T_{11}\lambda_m^2 + T_{12}\delta_n^2\right),$$
$$h_{42} = -\left(T_{13}\lambda_m^2 + T_{14}\delta_n^2 - n_{33}^*\right), h_{43} = -\left(T_{15}\lambda_m^2 + T_{16}\delta_n^2 - m_{33}^*\right),$$

$$o_{11}^* = \frac{1}{\rho_1}\left(\left(g_3\lambda_m^2 + f_3\delta_n^2\right)\phi_0 + \left(g_4\lambda_m^2 + f_4\delta_n^2\right)\psi_0 + \left(g_5\lambda_m^2 + f_5\delta_n^2\right)\Delta T\right),$$
$$o_{11} = \frac{-h_{11}}{\rho_1}, o_{12} = \frac{1}{\rho_1}\left(-h_{12} + g_1\lambda_m^2 + f_1\delta_n^2\right), \ o_{13} = \frac{-h_{13}}{\rho_1}, o_{14} = \frac{-h_{14}}{\rho_1},$$
$$o_{15} = \frac{-h_{15}}{\rho_1}, \ o_{16} = \frac{-h_{16}}{\rho_1}, \ o_{13}^* = \frac{\left(g_2\lambda_m^2 + f_2\delta_n^2\right)}{\rho_1},$$

$$T_{11} = -\int_{-h_f-h_c/2}^{-h_c/2} e_{31}z\beta\sin(\beta z)dz - \int_{h_c/2}^{h_c/2+h_f} e_{31}z\beta\sin(\beta z)dz,$$
$$T_{12} = -\int_{-h_f-h_c/2}^{-h_c/2} e_{32}z\beta\sin(\beta z)dz - \int_{h_c/2}^{h_c/2+h_f} e_{32}z\beta\sin(\beta z)dz,$$
$$T_{13} = \int_{-h_f-h_c/2}^{-h_c/2} \eta_{11}\cos^2(\beta z)dz + \int_{h_c/2}^{h_c/2+h_f} \eta_{11}\cos^2(\beta z)dz,$$
$$T_{14} = \int_{-h_f-h_c/2}^{-h_c/2} \eta_{22}\cos^2(\beta z)dz + \int_{h_c/2}^{h_c/2+h_f} \eta_{22}\cos^2(\beta z)dz,$$
$$T_{15} = \int_{-h_f-h_c/2}^{-h_c/2} m_{11}\cos^2(\beta z)dz + \int_{h_c/2}^{h_c/2+h_f} m_{11}\cos^2(\beta z)dz,$$
$$T_{16} = \int_{-h_f-h_c/2}^{-h_c/2} m_{22}\cos^2(\beta z)dz + \int_{h_c/2}^{h_c/2+h_f} m_{22}\cos^2(\beta z)dz,$$
$$\eta_{33}^* = -\int_{-h_f-h_c/2}^{-h_c/2} \eta_{33}\left(\beta\sin(\beta z)\right)^2 dz - \int_{h_c/2}^{h_c/2+h_f} \eta_{33}\left(\beta\sin(\beta z)\right)^2 dz,$$
$$m_{33}^* = -\int_{-h_f-h_c/2}^{-h_c/2} m_{33}\left(\beta\sin(\beta z)\right)^2 dz - \int_{h_c/2}^{h_c/2+h_f} m_{33}\left(\beta\sin(\beta z)\right)^2 dz.$$
$$T_{21} = -\int_{-h_f-h_c/2}^{-h_c/2} q_{31}z\beta\sin(\beta z)dz - \int_{h_c/2}^{h_c/2+h_f} q_{31}z\beta\sin(\beta z)dz,$$
$$T_{22} = -\int_{-h_f-h_c/2}^{-h_c/2} q_{32}z\beta\sin(\beta z)dz - \int_{h_c/2}^{h_c/2+h_f} q_{32}z\beta\sin(\beta z)dz,$$
$$\mu_{33}^* = -\int_{-h_f-h_c/2}^{-h_c/2} \mu_{33}\left(\beta\sin(\beta z)\right)^2 dz - \int_{h_c/2}^{h_c/2+h_f} \mu_{33}\left(\beta\sin(\beta z)\right)^2 dz$$
$$T_{23} = \int_{-h_f-h_c/2}^{-h_c/2} \mu_{11}\cos^2(\beta z)dz + \int_{h_c/2}^{h_c/2+h_f} \mu_{11}\cos^2(\beta z)dz,$$
$$T_{24} = \int_{-h_f-h_c/2}^{-h_c/2} \mu_{22}\cos^2(\beta z)dz + \int_{h_c/2}^{h_c/2+h_f} \mu_{22}\cos^2(\beta z)dz,$$